On the CMB large-scale angular correlations

Armando Bernui,[*] Thyrso Villela, Carlos A. Wuensche, Rodrigo Leonardi, and Ivan Ferreira

Instituto Nacional de Pesquisas Espaciais, Divisão de Astrofísica, Av. dos Astronautas 1758, 12227-010, São José dos Campos, SP – Brazil

e-mail: `bernui@das.inpe.br`

e-mail: `thyrso@das.inpe.br`

e-mail: `alex@das.inpe.br`

e-mail: `leonardi@das.inpe.br`

e-mail: `ivan@das.inpe.br`

Abstract. We study the large-scale angular correlation signatures of the Cosmic Microwave Background (CMB) temperature fluctuations from WMAP data in several spherical cap regions of the celestial sphere, outside the Kp0 or Kp2 cut-sky masks. We applied a recently proposed method to CMB temperature maps, which permits an accurate analysis of their angular correlations in the celestial sphere through the use of normalized histograms of the number of pairs of such objects with a given angular separation versus their angular separation. The method allows for a better comparison of the results from observational data with the expected CMB angular correlations of a statistically isotropic Universe, computed from Monte Carlo maps according to the WMAP best-fit ΛCDM model. We found that the, already known, anomalous lack of large-scale power in full-sky CMB maps are mainly due to missing angular correlations of quadrupole-like signature. This result is robust with respect to frequency CMB maps and cut-sky masks. Moreover, we also confirm previous results regarding the unevenly distribution in the sky of the large-scale power of WMAP data. In a bin-to-bin correlations analyses, measured by the full covariance matrix χ^2 statistic, we found that the angular correlations signatures in opposite Galactic hemispheres are anamalous at the 98%–99% confidence level.

Key words. Cosmology – large-scale structure of Universe – cosmic microwave background – anisotropies

1. Introduction

In recent years, after the COBE mission, experiments of observational cosmology evolved both in the accuracy and in the angular resolution of the Cosmic Microwave Background (CMB) measurements (see, e.g. Bersanelli et al. 2002 and references therein). However, such experiments were designed to map small patches of the celestial sphere and therefore the study of its properties concerning the large-scale angular correlations was not possible.

This situation changed with the Wilkinson Microwave Anisotropy Probe (WMAP), which produced full-sky CMB maps in five frequency bands (termed K, Ka, Q, V, and W maps), although containing different amounts of contaminations from our galaxy (Bennett et al. 2003a). This superb quality data set motivated a number of detailed studies concerning the CMB properties. As a result, several recent works have reported claims regarding

some anomalies found in these data. These anomalies include the low-order multipole values (Bennett et al. 2003a; Efstathiou 2004; Tegmark et al. 2003; Gaztañaga et al. 2003; Slozar et al. 2004; O'Dwyer et al. 2004), the alignment of some low-order multipoles (Tegmark et al. 2003; de Oliveira-Costa et al. 2004; Eriksen et al. 2004b; Bielewicz et al. 2005; Land and Magueijo 2005), and an unexpected asymmetric distribution on the sky of the large-scale power of CMB data (Eriksen et al. 2004a, 2005a; Hansen et al. 2004a, 2004b, 2004c; Jaffe et al. 2005; Schwarz et al. 2004; Copi et al. 2005).

In this work we focus on the study of the large-scale angular correlations (hereafter termed Angular Correlations Signatures ACS) of the CMB temperature maps from WMAP data. Since the vast majority of the cosmological information is contained in the two-point temperature correlation function, it seems natural to study the ACS by looking at such function (actually, an equivalent of it). Our analyses of the ACS in CMB maps, for data outside the region defined by the Kp0 or Kp2 WMAP masks, allow to perform a close inspection of two interesting issues. First, we investigate –through a full-sky map analysis– the large-scale power in WMAP data, and its connection with the low quadrupole moment issue. Second, we study

–through a partial-sky coverage analysis– the possible un-even distribution on the celestial sphere of the CMB large-scale power. The significance of our results are evaluated by comparing these results against those obtained from Monte Carlo CMB maps produced with the WMAP best-fitting ΛCDM model properties (Hinshaw et al. 2003b). Finally, using a χ^2 statistics we assess the confidence level of the North/South asymmetry in WMAP data compared to 1 000 Monte Carlo realizations of CMB skies.

2. Analyses method

Recently, Bernui & Villela (2006) introduced a new method to study the large-scale ACS in the distribution of cosmic objects in the sky. This method, called the Pair Angular Separation Histogram (PASH) method, consists in first calculating the angular distances between all pairs of cosmic objects, listed in a catalog, and then constructing the normalized histogram of the number of pairs with a given angular separation versus their angular separation. A catalog with a large number of objects can be divided in a number (say K) of comparable sub-catalogs (i.e. ensembles of iso-number of objects sharing analogous physical properties). After that, one computes a PASH with each one of these sub-catalogs and average them to obtain the Mean-PASH (MPASH). The difference between the MPASH, caculated using a observational catalog, and the Expected-PASH (EPASH), obtained assuming the statistical isotropy hypothesis (hereafter the MPASH-minus-EPASH function), shows the ACS of the cosmic objects in such a catalog.

In the CMB temperature maps the celestial sphere is partitioned in a set of equal-area pixels, where to each pixel is assigned a weighted CMB temperature. To obtain the ACS of a given map, one divides the set of pixels in $K = 2$ sub-maps, one for the negative CMB temperature fluctuations and the other for the positive ones, and proceeds as before averaging ($K =$) 2 PASHs. If, for computational problems, the number of pixels in these sub-maps is too large, one can divide them in, say K_- and K_+, sub-maps (with iso-number of pixels of analogous temperatures), and proceeds to compute the MPASH averaging the $K = K_- + K_+$ PASHs, and finally, one plots the MPASH-minus-EPASH function. It can be shown (see Bernui 2005) that the MPASH-minus-EPASH function is independent of the number of sub-maps $K_- \geq 1$ and $K_+ \geq 1$ in which the original CMB map is divided.

The PASH method is also applicable to incomplete sky maps, including disconnected regions such as those resulting from the application of the WMAP masks. This method is similar in philosophy to the two-point temperature correlation function, except that the PASH method has zero mean, because the MPASH and EPASH are each one normalized histograms. This simple fact allows us to achieve a deeper study of the ACS in CMB temperature maps, like: the intensity of all their relative mimima and maxima and their corresponding angular scales, their intersections with the horizontal axis (i.e. the zeros of the

function), etc; it also leads to calculate the variance σ^2 of the MPASH-minus-EPASH function f_i (which has zero mean, i.e., $\sum_{i=1}^{N_{\mathrm{bins}}} f_i = 0$)

$$\sigma^2 = \frac{1}{N_{\mathrm{bins}}} \sum_{i=1}^{N_{\mathrm{bins}}} f_i^2 \ .$$

3. CMB data analyses

In this section we present the ACS of the WMAP data. For these analyses, we used six CMB maps: the individual Q-, V-, and W-band data produced from the (Q_1,Q_2), (V_1,V_2), and (W_1,W_2,W_3, W_4) differential assemblies (DA), respectively, as provided on LAMBDA [1] (Bennett et al. 2003b), the COADDED WMAP map (which combines the eight DA in the Q-, V-, and W-bands using the inverse-variance noise weights as described by Hinshaw et al. (2003b)), the *cleaned* CMB map (Tegmark et al. 2003, hereafter the TOH map), and the Lagrange Internal Linear Combination (Eriksen et al. 2004b, hereafter the LILC map). It is known that the last two maps are not fully reliable for quantitative analysis because still have problems with residual foregrounds (Eriksen et al. 2005b); here we use them just as a supporting evidence. After applying the Kp0 or Kp2 WMAP masks in all these six maps, we remove their residual monopole and dipole components, and correct them for the dynamic quadrupole.

The examination of the WMAP data performed here comprehends two types of sky analyses. We want to remark that in both cases we consider data outside the region defined by the Kp0 or the Kp2 mask, to avoid from the beginning residual foreground contaminations (Bennett et al. 2003b; Eriksen et al. 2004b, 2005b; Bielewicz et al. 2004). The first type is the full-sky analysis, and the second one is the partial-sky analysis carry out through antipodal spherical caps of $45°$, $60°$, and $90°$ of aberture (this means that the maximum angular separation between pixels in each case is twice these angle values).

We use CMB maps with HEALPix (Górski et al. 2005) resolution $N_{\mathrm{side}} = 128$, which amounts to 196 608 pixels. In the following figures we consider the bin width as $0.45°$, and the number of bins as $N_{\mathrm{bins}} = 400$; moreover, the shaded areas correspond to 1-sigma confidence regions.

3.1. Full-sky analyses (outside Kp2 or Kp0 masks)

In this subsection we shall discuss the ACS of the WMAP maps, analysing the CMB data outside the regions defined by the Kp2 and Kp0 masks. The objective of such analysis is to investigate previous claims regarding the lack of power in the large-scale angular correlations in full-sky data (see Bennett et al. 2003a; Efstathiou 2004; Slosar et al. 2004) and its relationship to the low-order multipole values.

---

[1] http:\\lambda.gsfc.nasa.gov\product\map\current\IMaps$_-$cleaned.cfm

First we show the ACS of the WMAP data using the Kp2 mask. In fact, the suitability of using each WMAP mask is well known in the literature, and many works claim that the less severe cut-sky Kp2 could be enough for cosmological purposes (large angular scales). We have computed the ACS for both masks, although we only show the ACS for the Kp2 mask case, and for all maps under investigation to assert the robustness of our results under different sky cuts.

The results are reported in Figure 1. In the top panel of Fig. 1 we show the ACS from the six CMB maps here investigated, considering data outside the region determined by the Kp2 mask. For comparison we also plot, as a dashed line, the average of 1 000 MPASH-minus-EPASH functions (termed the *expected function*) obtained from the same number of Monte Carlo CMB maps. These realizations were produced using an input power spectrum generated by the CMBFAST code (Seljak & Zaldarriaga 1996) considering the WMAP best-fitting ΛCDM model properties. The maps were produced using the map-making code SYN-FAST from HEALPix. The disagreement observed between the observational data from WMAP and the expected angular correlation function is better appreciated in the bottom panel of Fig. 1, where we plotted the difference of such expected function minus each one of the MPASH-minus-EPASH functions from the six CMB maps. What is revealed in these difference plots is that the ACS missing in CMB data at large-angular scales correspond to a quadrupole-like angular correlation signature (see, e.g., Bernui 2005). To assess this, we plot the angular correlation function of a quadrupole (corrected for the Kp2 mask) with moment $C_2 \simeq 670\mu\mathrm{K}^2$. Since these curves (bottom panel Fig. 1) represent the missing ACS in WMAP data to fit the expected function, where $C_2^{\Lambda\mathrm{CDM}} = 870\mu\mathrm{K}^2$, one finds $C_2^{\mathrm{WMAP}} \simeq 190 \pm 30\mu\mathrm{K}^2$, that are in good agreement with Bielewicz et al. (2004) who obtained $C_2 = 165 \pm 34, 216 \pm 42, 229 \pm 44, 191 \pm 38 \,\mu\mathrm{K}^2$, for the Q, V, W, and Coadded maps, respectively). This result, which appears to be robust with respect to the frequency CMB map and to cut-sky mask (we also performed analyses with the Kp0 mask obtaining similar results), proves that the lack of angular power previously found in the two-point temperature correlation function of WMAP data is mainly due to the low quadrupole moment (Efstathiou 2004; Gaztañaga et al. 2003; Slosar et al. 2004).

Furthermore, to confirm this result we remove the quadrupole component, after applying the Kp2 mask, and compute the ACS in these maps. The result is shown in Figure 2 where we also plot for comparison the expected function for the case of zero quadrupole component. Again this result is robust with respect to the frequency CMB map analyzed.

3.2. Partial-sky analyses

The basic idea is to investigate different regions of the celestial sphere, namely spherical caps of various sizes, whose
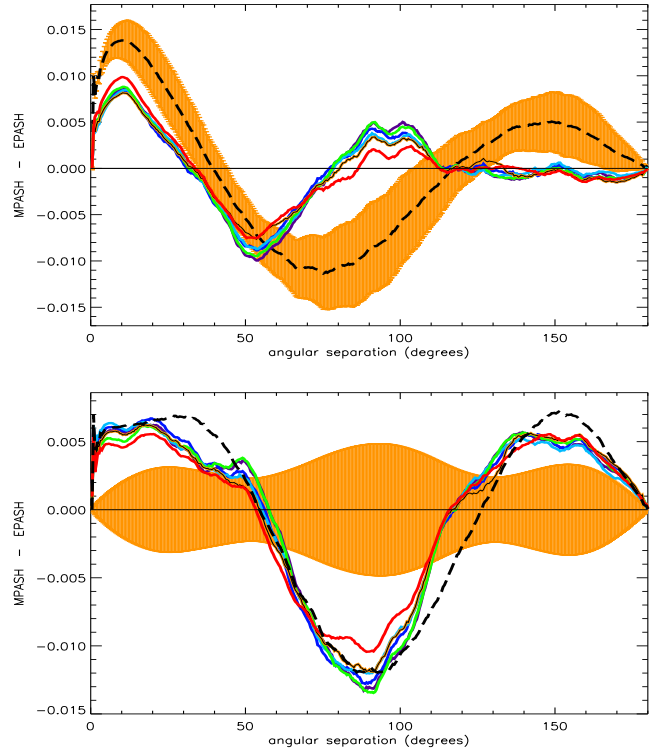

Fig. 1. Top panel: ACS in the six CMB maps: Q (violet line), V (blue line), W (light-blue line), Coadded (green line), TOH (brown line), and LILC (red line), after applying the Kp2 mask. For comparison we also plot the average of 1 000 MPASH-minus-EPASH functions obtained from the same number of Monte Carlo CMB maps (dashed line, also called the expected function). One unit in the vertical axis corresponds to $5\,460\mu\mathrm{K}^2$. Bottom panel: The differences of the expected function minus the six MPASH-minus-EPASH functions from the top panel, where we observe that these ACS correspond mainly to a quadrupole-like signature. The dashed line here corresponds to the MPASH-minus-EPASH of a quadrupole (corrected for the Kp2 mask) with $C_2 \simeq 670\mu\mathrm{K}^2$. Notice that these curves represent the missing ACS in WMAP data to fit the expected function, which have $C_2^{\Lambda\mathrm{CDM}} = 870\mu\mathrm{K}^2$.

vertices point in the direction of the North Galactic Pole (NGP) and the South Galactic Pole (SGP), with respect to the Galactic coordinate system. Comparison of the ACS in antipodal caps of 45°, 60°, and 90° of aberture allows a quantitative assessement of the claimed asymmetry in the distribution of the CMB power between the northern and southern hemispheres (Eriksen et al. 2004b).

The resulting ACS are shown in Figures 3 and 4, where the expected functions result from data on the same patch of the sky from Monte Carlo CMB maps. In Figure 3 we present four plots: panels (a) and (b) reveal the ACS in the 45° NGP-cap and SGP-cap, respectively; while in panels (c) and (d) we show the ACS in the 60° NGP-cap and SGP-cap, respectively. In Figure 4, we also show four plots: panels (a) and (b) reveal the ACS in the 90°-cap, outside the Kp2 mask, in the Northern and Southern
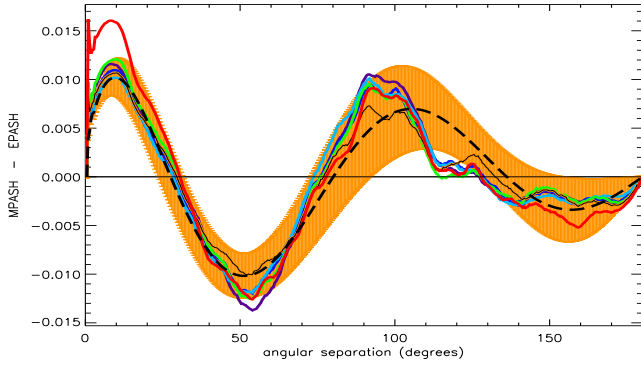
Fig. 2. The ACS for the six CMB maps (the nomenclature of the curves follows the same color's pattern as before) with the quadrupole component removed. The dashed line is the expected function for the case of zero quadrupole moment.

Galactic hemispheres (NGH, SGH), respectively; panels (c) and (d) show the ACS in the 90°-cap, outside the Kp2 mask, in the NGH and SGH, respectively, but this time we removed the quadrupole component of the CMB maps.

Some interesting features in these plots are evident. The first noticeable result is that, in each one of these figures the ACS corresponding to the three frequency maps Q, V, and W are practically indistinguishable. It is well known (see Bennett et al. 2003b) that foregrounds have a frequency-band dependence, thus when incorrectly subtracted it is expected to show up at a different level in the frequency maps Q, V, and W. To investigate the robustness of our results with respect to a different sky cut, we computed the ACS for the NGH and SGH (not shown here) for data outside the more severe galactic cut given by the WMAP Kp0 mask (it cuts ∼ 25% of the total data, while the Kp2 mask cuts ∼ 15%), where we found similar results. Thus, one concludes that the ACS found in these maps are remarkably stable with respect to both frequency bands and sky cuts, and seem unlikely to be compromised by residual foregrounds.

The second interesting fact is the net asymmetry between the 90°-caps in NGH and SGH: the Northern hemisphere is almost structureless (the variance's square-root for this ACS is $\langle\sigma_N^{\mathrm{Q,V,W}}\rangle = 0.0054$ while $\sigma^{\mathrm{Expected}} = 0.012 \pm 0.006$), instead the ACS in the Southern hemisphere are relatively intense ($\langle\sigma_S^{\mathrm{Q,V,W}}\rangle = 0.016$ while $\sigma^{\mathrm{Expected}} = 0.015 \pm 0.008$). In this form, the South/North ratio $\sigma_{S/N} \equiv \sigma_S/\sigma_N = 2.97$ quantifies the evident SGH/NGH asymmetry observed in the plots of figure 4. The statistical significance of this result are evaluated in the next section, by means of the Monte Carlo maps, in terms of the standard covariance matrix χ^2 statistic.

Finally, in order to check the possibility that the low value of the quadrupole moment could be responsible for this peculiar ACS behavior, we removed the quadrupole component, after applying the Kp2 mask, in all the six maps, and then compute again the MPASH-minus-EPASH for data in the 90°-caps in the NGH and SGH.

Our results can be seen in the Figures 4c and 4d, where this time $\langle\sigma_N^{\mathrm{Q,V,W}}\rangle = 0.0065$ in the NGH, and $\langle\sigma_S^{\mathrm{Q,V,W}}\rangle = 0.019$ in the SGH. The large value now obtained for the ratio $\sigma_{S/N} = 2.96$, confirms that the North/South asymmetry is not related to the low quadrupole value.

A natural question concerns the frequency that such a ratio is $\sigma_{S/N} \simeq 3$ ($\sigma_{S/N} = 3.2$ if data from Coadded map is included in the average) is present in the ensemble of Monte Carlo maps. Analysing the MPASH-minus-EPASH functions for similar NGH and SGH 90°-caps in 1 000 Monte Carlo maps, we found that the corresponding values of $\sigma_{S/N} \in [0.2, 5.4]$, with mean $\sigma_{S/N}^{\mathrm{mean}} = 1.1 \pm 0.7$. A close inspection of the values in such interval results in that less than 2% of them satisfies $\sigma_{S/N} > 3$.

4. Statistical analyses

In this section we present the statistical analysis of the ACS obtained from WMAP data against analogous results derived from the 1 000 Monte Carlo CMB maps. The degree of agreement between the simulations and the observations are quantified in terms of a standard covariance matrix χ^2 statistic, including all bin-to-bin correlations,

$$\chi^2 = \sum_{i,j=1}^{N_{\mathrm{bins}}} (f_i - \langle f_i\rangle) M_{ij}^{-1}(f_j - \langle f_j\rangle),$$

where $\langle f_i\rangle$ is the mean of the MPASH-minus-EPASH functions as determined by the Monte Carlo maps, and $M_{ij} \equiv \langle f_i f_j\rangle - \langle f_i\rangle\langle f_j\rangle$ is the covariance matrix. The results from these computations, divided in three groups for the 45°-, 60°-, and 90°-caps, respectively, are reported in Table 1. The first column indicates the CMB map investigated, the second and third ones indicate the frequencies of Monte Carlo simulations with a lower χ^2 value than the WMAP data for the NGH and SGH, respectively. The last column indicates the frequency of simulations with a smaller $\chi^2_{\mathrm{SGP}}/\chi^2_{\mathrm{NGP}}$. These results determine a parameter, the ratio of the χ^2 values for the NGH and SGH, that is used to quantify the degree of asymmetry between both hemispheres (Eriksen et al. 2004a, 2005a).

The results reported in Table 1 are as follows. In all the cases, the NGH and SGH show, indepedently, acceptable values of probability (frequency of simulated maps, given the model, where the MPASH-minus-EPASH function of such maps has a lower χ^2 value than the WMAP data). However, data in the third column says that the antipodal 90°-caps are marginally consistent internally (when considered simultaneously one as opposite to the other): for the Q, V, W, and Coadded maps the mean of the $\chi^2_{S/N}$ values is $\gtrsim 0.98$, or equivalently $\chi^2_{N/S} \lesssim 0.02$, which means that $\lesssim 2\%$ of the simulations have a smaller ratio of χ^2. It is worth to notice that these results appearing in the 90°-caps are shown to be robust with respect to frequency (the same result for Q, V, W, and Coadded CMB maps). Therefore, we conclude that there is a significant discrepancy, at the $\gtrsim 98\%$ CL, between WMAP data and the ACS expected in a statistically isotropic Universe.

Table 1. χ^2-test for the ACS in different caps. The first column indicates the CMB map investigated, the second and third ones indicate the frequency of Monte Carlo simulations with a lower χ^2 value than the WMAP data. The last column indicates the frequency of simulations with a smaller $\chi^2_{\text{SGH}}/\chi^2_{\text{NGH}}$.

CMB map	χ^2−NGH	χ^2−SGH	$\chi^2_{S/N}$
45°			
Q	0.914	0.891	0.499
V	0.854	0.902	0.624
W	0.654	0.782	0.616
COADDED	0.969	0.967	0.548
TOH	0.865	0.759	0.419
LILC	0.817	0.882	0.626
60°			
Q	0.715	0.971	0.949
V	0.637	0.982	0.956
W	0.361	0.959	0.930
COADDED	0.550	0.909	0.822
TOH	0.786	0.926	0.712
LILC	0.154	0.884	0.891
90°			
Q	0.276	0.959	0.985
V	0.243	0.810	0.965
W	0.278	0.968	0.976
COADDED	0.143	0.929	0.990
TOH	0.164	0.724	0.846
LILC	0.176	0.770	0.853

5. Conclusions

Here we have shown through the full-sky analyses of the ACS of the WMAP data (outside the Kp0 or Kp2 sky cuts) that the 'anomalous' lack of power at large angular scales is mainly explained by the low quadrupole-moment value (see Efstathiou 2004, Gaztañaga et al. 2003, and Slosar et al. 2004 for more detailed discussions; see also Bielewicz et al. 2004 for complete calculations, in particular in similar band maps as here). We confirmed this result by analysing also the WMAP data after removing the quadrupole component, obtaining a better (but not exactly) agreement with what is expected in a ΛCDM model with zero quadrupole.

We also performed partial-sky coverage analyses and showed that there is significative evidence, at the $98\% - 99\%$ CL, of an anomalous distribution of the CMB power in opposite Galactic hemispheres. In fact, in less than 2% of the Monte Carlo CMB maps analyzed, data in opposite hemispheres present analogous bin-to-bin correlations as those shown by the 90°-caps with WMAP data. More interestingly, the excess of correlations in the comparison of opposite antipodal caps is manifestly observed in the South/North 90°-caps, but it is not seen neither in the examination of the antipodal 45°- or 60°-caps.

The fact that the South/North asymmetry persists at a significant level in several frequency bands (the Q, V, and W CMB maps) and with different sky cuts (the Kp0 and Kp2 masks) excludes a simple explanation based on systematic effects and foregrounds (see Hinshaw et al. 2003a; Eriksen et al. 2004a, 2004b; Hansen et al. 2004b).

References

Bennett, C. L., Halpern, M., Hinshaw, G., et al. 2003a, ApJS, 148, 1

Bennett, C. L., Hill, R. S., Hinshaw, G., et al. 2003b, ApJS, 148, 97

Bernui, A. & Villela, T. 2006, A&A, 445, 795; astro-ph/0511339

Bernui, A. 2005, astro-ph/0511592

Bersanelli, M., Maino, D., & Mennella, A. 2002, Rivista del Nuovo Cimento, 25, N.9, 1

Bielewicz, P., Gorski, K. M., & Banday, A. J. 2004, MNRAS, 355, 1283

Bielewicz, P., Eriksen, H. K., Banday, A. J., Górski, K. M., & Lilje, P. B. 2005, astro-ph/0507186

Copi, C. J., Huterer, D., Schwarz, D. J., & Starkman, G. D. 2005, astro-ph/0508047

de Oliveira-Costa, A., Tegmark, M., Zaldarriaga, M., & Hamilton, A. J. S. 2004, Phys. Rev. D, 69, 063516

Efstathiou, G. 2004, MNRAS, 348, 885

Eriksen, H. K., Hansen, F. K., Banday, A. J., Górski, K. M., & Lilje, P. B. 2004a, ApJ, 605, 14; Errat. 2004, 609, 1198

Eriksen, H. K., Banday, A. J., Górski, K. M., & Lilje P. B. 2004b, ApJ, 612, 633

Eriksen, H. K., Banday, A. J., Górski, K. M., & Lilje P. B. 2005a, ApJ, 622, 58

Eriksen, H. K., Banday, A. J., Górski, K. M., & Lilje P. B. 2005b, astro-ph/0508196

Gaztañaga, E., Wagg, J., Multamäki, T., Montaña, A., & Hughes, D. H. 2003, MNRAS, 346, 47

Górski, K. M., Hivon, E., Banday, A. J., et al. 2005, ApJ, 622, 759

Hansen, F. K., Cabella, P., Marinucci, D., & Vittorio, N. 2004a, ApJ, 607, L67

Hansen, F. K., Banday, A. J., & Górski, K. M. 2004b, MNRAS, 354, 641

Hansen, F. K., Balbi, A., Banday, A. J., & Górski, K. M. 2004c, MNRAS, 354, 905

Hinshaw, G., Barnes, C., Bennett, C. L., et al. 2003a, ApJS, 148, 63

Hinshaw, G., Spergel, D. N., Verde, L., et al. 2003b, ApJS, 148, 135

Jaffe, T. R., Banday, A. J., Eriksen, H. K., Gorski, K. M., & Hansen, F. K. 2005, ApJ, 629, L1

Land, K. & Magueijo, J. 2005, Phys. Rev. Lett., 95, 071301

O'Dwyer, I. J., Eriksen, H. K., Wandelt, B. D., et al. 2004, ApJ, 617, L99

Seljak, U. & Zaldarriaga, M. 1996, ApJ, 469, 437

Slosar, A., Seljak, U., & Makarov, A. 2004, Phys. Rev. D, 69, 123003

Schwarz, D. J., Starkman, G. D., Huterer, D., & Copi, C. J. 2004, Phys. Rev. Lett., 93, 221301

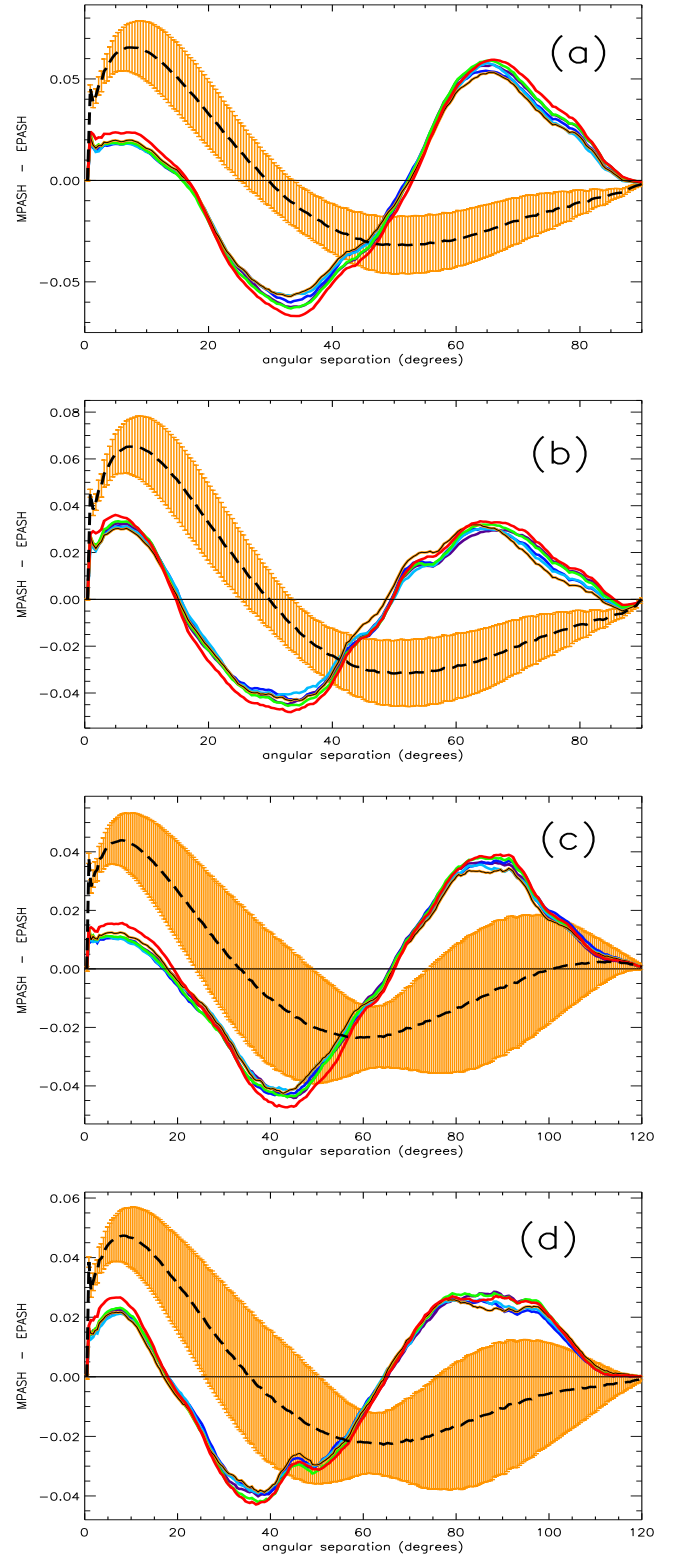Tegmark, M., de Oliveira-Costa, A., & Hamilton, A. J. S. 2003, Phys. Rev. D, 68, 123523

Fig. 3. The ACS in the 45°-caps in the NGH (a) and in the SGH (b), and the ACS in the 60°-caps in the NGH (c) and in the SGH (d), from the six CMB maps (Q, V, W, Coadded, TOH, and LILC), after applying the Kp2 mask. In all plots the dashed line is the average of MPASH-minus-EPASH functions obtained from the corresponding sky regions in 1 000 Monte Carlo maps, respectively. The nomenclature of the curves follows the same color's pattern as in Figure 1.
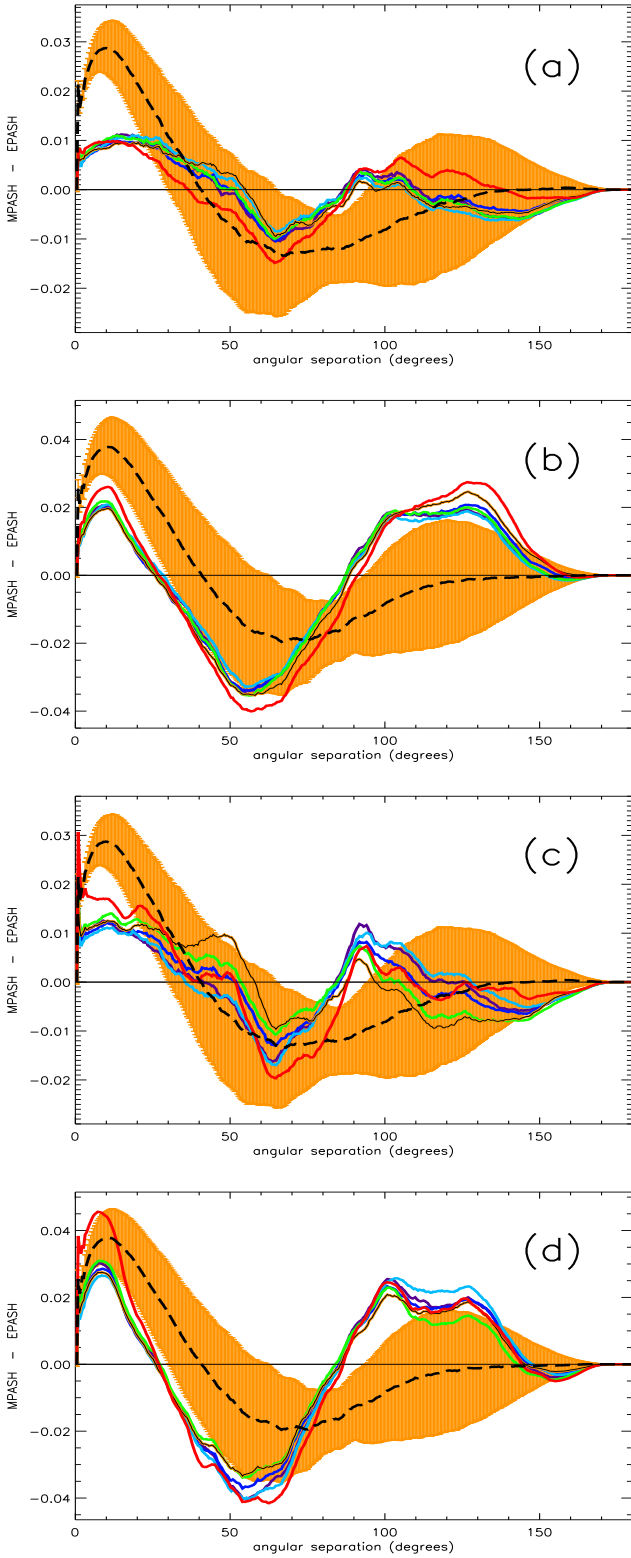
Fig. 4. The ACS in the 90°-caps in the NGH (a) and in the SGH (b), from the six CMB maps (Q, V, W, Coadded, TOH, and LILC), after applying the Kp2 mask. Removing the quadrupole component, after applying the Kp2 mask, in the six CMB maps we obtain the ACS in the 90°-caps in the NGH (c), and in the SGH (d). For comparison, the dashed line and the shaded region in panel (a) (panel (b)) is the same as in panel (c) (panel (d)). As before, the nomenclature of all the curves follows the same color's pattern as in Figure 1.